

# The Role of Zonal Asymmetry in the Enhancement and Suppression of Sudden Stratospheric Warming Variability by the Madden–Julian Oscillation

WANYING KANG

*School of Engineering and Applied Sciences, Harvard University, Cambridge, Massachusetts*

ELI TZIPERMAN

*Department of Earth and Planetary Sciences, and School of Engineering and Applied Sciences, Harvard University, Cambridge, Massachusetts*

(Manuscript received 21 July 2017, in final form 19 December 2017)

## ABSTRACT

Sudden stratospheric warming (SSW) events influence the Arctic Oscillation and midlatitude extreme weather. Previous work showed the Arctic stratosphere to be influenced by the Madden–Julian oscillation (MJO) and that the SSW frequency increases with an increase of the MJO amplitude, expected in a warmer climate. It is shown here that the zonal asymmetry in both the background state and forcing plays a dominant role, leading to either enhancement or suppression of SSW events by MJO-like forcing. When applying a circumglobal MJO-like forcing in a dry dynamic core model, the MJO-forced waves can change the general circulation in three ways that affect the total vertical Eliassen–Palm flux in the Arctic stratosphere. First, weakening the zonal asymmetry of the tropospheric midlatitude jet, and therefore preventing the MJO-forced waves from propagating past the jet. Second, weakening the jet amplitude, reducing the waves generated in the midlatitudes, especially stationary waves, and therefore the upward-propagating planetary waves. Third, reducing the Arctic lower-stratospheric refractory index, which prevents waves from upward propagation. These effects stabilize the Arctic vortex and lower the SSW frequency. The longitudinal range to which the MJO-like forcing is limited plays an important role as well, and the strongest SSW frequency increase is seen when the MJO is located where it is observed in current climate. The SSW suppression effects are active when the MJO-like forcing is placed at different longitudinal locations. This study suggests that future trends in both the MJO amplitude and its longitudinal extent are important for predicting the Arctic stratosphere response.

## 1. Introduction

Major sudden stratospheric warming (SSW) events occur in the Arctic stratosphere during winter at a frequency of about six events per decade. An SSW features a distorted or completely reversed stratospheric polar vortex, as well as tens of degrees warming within several days (Craig et al. 1959; Limpasuvan et al. 2004). In the month following an SSW event, the Northern Hemisphere is more likely to be in the negative phase of the Arctic Oscillation (AO)/northern annular mode (NAM), and also to experience more extreme weather (Thompson et al. 2002; Kolstad et al. 2010; Mitchell et al. 2013). Also, the high temperature in the Arctic stratosphere associated with SSWs may prohibit the formation

of polar stratospheric clouds and reduce stratospheric ozone depletion (Solomon et al. 1986). Some general circulation model (GCM) studies found an increased frequency of SSWs in future climate projections (Schimanke et al. 2013; Bell et al. 2010; Charlton-Perez et al. 2008; Kim et al. 2017), although these results seem inconclusive (Butchart et al. 2000; McLandress and Shepherd 2009; Mitchell et al. 2012). A better understanding of the trend of SSW frequency in a future climate could help predict expected trends in midlatitude winter weather.

Vertically propagating planetary waves play an important role in SSW dynamics (Matsuno 1971; Holton and Mass 1976), and SSW events are observed to be preceded by various phenomena that could lead to such waves, including midlatitude blocking systems (Martius et al. 2009; Bancalá et al. 2012), tropospheric quasi-stationary waves (Cohen and Jones 2011), and strong

---

*Corresponding author:* Wanying Kang, wanyingkang@g.harvard.edu

polar vortex events (Limpasuvan et al. 2004). SSW events are also observed to be related to tropical variability, including the quasi-biennial oscillation (QBO; Holton and Tan 1980) and the Madden–Julian oscillation (MJO; Garfinkel et al. 2014, 2012; Kang and Tziperman 2017, hereafter KT17). Specifically, KT17 showed that an increase in the MJO amplitude, expected in a global warming scenario (Arnold et al. 2014) leads to an increased SSW frequency. In this paper we further examine the MJO–SSW teleconnection mechanism, and specifically the role of zonal asymmetry both of the background state and of the MJO-like forcing, and analyze the mechanisms involved.

The MJO (Madden and Julian 1971; Zhang 2005) was shown in both reanalysis and simulations to be related to high-latitude tropospheric variability, including Northern Hemisphere blocking, stronger upward Eliassen–Palm (EP) flux in the midlatitudes, the Pacific–North American (PNA) pattern, a warmer Arctic surface (Yoo et al. 2012b, 2011, 2012a; Cassou 2008), and also a weakened polar vortex (Goss et al. 2016). Given that the MJO was shown, in both models and observations, to be strengthened (Slingo et al. 1999; Jones and Carvalho 2006; Lee 1999; Arnold et al. 2013, 2014; Chang et al. 2015), and to occupy a larger longitudinal range (Chang et al. 2015) in a warmer climate, a better understanding of the teleconnection between the MJO and the SSW frequency is important for predicting future SSW frequency trends, and for predicting changes in midlatitude extreme weather frequency, stratospheric ozone recovery, and more.

KT17 showed that Rossby wave trains excited by MJO phases 3–5 propagate northward, then upward, to the Arctic stratosphere within one month, and as a result, that stronger MJO forcing can nearly double the SSW frequency. They noticed a northward wave train departing from the tropics in MJO phases 3–5, which corresponds to enhanced convection near Indonesia. In observations, Garfinkel et al. (2014) found that the MJO effect on the average polar cap temperature also occurs preferentially after MJO phases 3 and 7; and Schwartz and Garfinkel (2017) noted that more than half of SSWs occur after MJO phase 6/7 (other studies have found that MJO-related convection in other phases can also impact the extratropics; Goss and Feldstein 2017). These results imply that the MJO-forced waves may propagate only at certain longitudes, which can either be a result of the different forcing structure associated with different MJO phases, or because of the interaction with the background zonal asymmetry. In this work, we demonstrate the second effect by forcing a model with an idealized wavenumber-1 MJO-like forcing.

Indeed, the zonal asymmetry involved with background wind convergence associated with the jet exit

regions, located in the east Pacific and Atlantic, was shown to help the amplification, accumulation, and propagation of Rossby waves when propagating from the tropics to higher latitudes (Simmons et al. 1983; Branstator 1985; Webster and Chang 1988; Naoe et al. 1997; Hoskins and Jin 1991; Bao and Hartmann 2014). Consistently, previous work also showed that the zonal asymmetry of the basic flow affects the emanation and propagation of equatorial waves from the tropics, especially when nonlinear effects are important (Jin and Hoskins 1995; Naoe and Matsuda 1998).

In this paper, we perform dry dynamic core experiments forced with a range of MJO amplitudes, using configurations with and without zonal asymmetry in the prescribed background state, and varying the longitudinal extent and location of the MJO forcing, to study the effect of increasing MJO amplitude and longitudinal extension. We use a range of MJO-forcing characteristics that include, but are not limited to, the realistic parameter range. In particular, we adopt very strong amplitude forcing to explore the mechanism in a larger parameter regime, as well as circumglobal forcing to isolate the effect of background zonal asymmetry.

We show that the response of the Arctic stratosphere, and in particular that of the SSW frequency, critically depends on the zonal asymmetry of the background state and the longitudinal extent of the MJO forcing: first, a zonally symmetric background state does not allow the MJO signal to propagate to the Arctic stratosphere; second, a circumglobal forcing, propagating in a realistic zonally asymmetric background state, increases the SSW frequency at low MJO amplitudes and suppresses it at larger amplitudes; third, an MJO forcing restricted to the observed Indo-Pacific section leads to a warming of the Arctic stratosphere, and enhances the variability there, in a very wide range of MJO amplitudes; fourth, longitudinally restricted MJO forcings at different locations have significant different effects on the Arctic stratosphere.

The mechanism leading to the suppression of SSW variability is shown to be due to several factors that reduce the wave activity seen by the Arctic stratosphere, and thus stabilize it: 1) the reduction in zonal asymmetry of the tropospheric jets, caused by a nonlinear interaction with the MJO-forced waves, reduces the poleward propagation of the MJO-forced waves; 2) the midlatitude jet, weakened through absorption of MJO-forced waves, generates less upward-propagating waves, in particular stationary waves, and gives rise to less total EP<sub>z</sub> entering the Arctic stratosphere; and 3) the lower-stratospheric planetary wave refraction index is modified by the reduction of upward EP flux, further

TABLE 1. Model runs used in this study. All zonally asymmetric experiments were run for 100 years, zonally symmetric experiments (denoted by 2d in the table) were run for 50 years. When labeled with “Win,” the longitudinal range of the MJO forcing to is restricted to 60°E–180° by default, or as specified otherwise. The [S]% and [S]% + topo runs only appear in the context of Fig. 6, see section 2 for further details of model configuration.

| Name        | Description                                                        |
|-------------|--------------------------------------------------------------------|
| CTRL        | Unforced, January climatology                                      |
| MJO[N]      | CTRL with added MJO-forcing amplitude of [N] K day <sup>-1</sup>   |
| MJO[N]Win   | MJO forcing restricted to longitudinal window                      |
| 2dCTRL      | Unforced, zonally symmetric January climatology, no topography     |
| 2dMJO[N]    | 2dCTRL with added MJO-forcing amplitude of [N] K day <sup>-1</sup> |
| [S]% + topo | [S]% of background zonal asymmetry retained, with topography       |
| [S]%        | As in [S]% + topo, but with a flat topography                      |

preventing the upward propagation, again reducing the wave activity in the Arctic stratosphere.

The following section presents the structure of the MJO forcing used as well as the idealized model configurations used. Section 3 describes the results for a range of MJO-forcing amplitudes, with and without zonal asymmetry in the background state and in the MJO-like forcing, and proposes a mechanism for the responses seen. We present our conclusions in section 4.

## 2. Methods

### a. Idealized model configuration

The idealized model experiments used here are configured following Held and Suarez (1994), based on the idealized physics component set in the Community Earth System Model, version 1.2.2 (CESM; Neale et al. 2010), replacing radiation, convection, and other physics processes by a restoring term to an equilibrium temperature  $T_{eq}$  with a time scale set to 40 days above 850 mb (1 mb = 1 hPa). Surface friction is represented by strongly restoring  $U$ ,  $V$ , and  $T$  in the bottom three layers toward the equilibrium state with 4-day time scale. The finite-volume core is used, and the horizontal resolution is 1.875° in latitude and 2.5° in longitude. We use the bottom 35 pressure–sigma hybrid layers from the standard Whole Atmosphere Community Climate Model (WACCM), with the model top located at 3 mb. Of these, 18 layers are in the stratosphere, which guarantees the vertical resolution is finer than 2 km everywhere and that SSW events are reasonably simulated (Richter et al. 2014). The control run SSW frequency is as observed, although this may be a coincidence, given that previous low-top models struggled to simulate a realistic SSW frequency (Charlton-Perez et al. 2013). To avoid numerical instability caused by wave reflection at the model top, the temperature restoring time scale is

gradually reduced from 40 to 30 days over the top four layers, at pressure levels of 6 mb and above. We thus expect the model response above 6 mb to the MJO forcing to be slightly damped. To study the MJO–SSW teleconnection in a “realistic” background state, we use a realistic topography, and add a static forcing to reproduce the  $U$ ,  $V$ , and  $T$  climatology in the January of a  $1 \times \text{CO}_2$  specified chemistry WACCM run, using the method of Hall (2000). A total of 800 one-step simulations are started from instantaneous meteorological states taken from the January states of a WACCM run. The averaged negative of the time tendency (the  $U$ ,  $V$ , and  $T$  at time step 0 minus those at time step 1) is then used as an extra static forcing of the prognostic variables. This forcing thus nudges the model state toward the WACCM January initial conditions. The use of an average over multiple initial conditions leads to a nudging toward the January climatology of WACCM, representing missing physics in the idealized model, including eddy fluxes, and making sure that the idealized model climatology is as consistent with the WACCM January climatology as possible. The zonally symmetric background state used below is set by removing the topography and using the zonal mean of the realistic case forcing terms. The zonal-mean climatology of the realistic and zonally symmetric cases are nearly identical.

To investigate how the background zonal asymmetry affects the transmission of MJO-forced waves [section 3b (2)], we modify the amplitude of the background state zonal asymmetry by applying a factor of 0%, 20%, 50%, 80%, and 100% to the asymmetric component of the abovementioned static forcing (the negative time tendency of  $U$ ,  $V$ , and  $T$ ). We then run the simulations with no MJO forcing and with the 2 K day<sup>-1</sup> circumpolar MJO-like forcing to isolate the effect of the background zonal asymmetry. In addition, we also run these experiments with a flat topography to study the role played by topography alone. These experiments are named [S]% + topo and [S]%, respectively, as summarized in Table 1.

### b. MJO forcing

MJO-like forcing is added to the idealized model as an external heating source, with a zonal wavenumber-1 structure, and a period of  $2\pi/\omega = 40$  days. The adiabatic heating structure is given by

$$H = A \exp\left(-\frac{\sin^2\phi}{2\sigma_y^2}\right) \sin(k\lambda - \omega t) \cos\left[\frac{\log(p_0/p)}{\log(p_{\text{surf}}/p_0)} \frac{\pi}{2}\right] \times W(\lambda), \quad (1)$$

where  $\sigma_y = 5^\circ$ ,  $k$  is the forcing zonal wavenumber, and  $A$  is the heating amplitude, set in the different experiments below to 0, 1, 2, 3, 4, 5, 6, 7, and  $10 \text{ K day}^{-1}$ . When specified, this forcing is limited to a longitudinal range using a tanh-based window function  $W(\lambda)$ . Note that, with or without longitudinal restriction, the forcing has zero net heating everywhere after taking time average. The experiments are run for 100 years and are summarized in Table 1.

We note that an MJO forcing with over  $3 \text{ K day}^{-1}$  heating rate is not realistic in the current climate, and  $7\text{--}10 \text{ K day}^{-1}$  forcing, as used in our experiments, may be too strong even for a very warm past or future climate. Therefore, these strongly forced experiments are meant to help us understand the teleconnection mechanisms in a wide parameter regime, hopefully providing insights that put our understanding of the more realistic regime in perspective. In addition, the MJO forcing itself is used either as a propagating circumglobal signal with a zonally uniform amplitude, or being restricted to a zonal window. By applying (unrealistic) circumglobal MJO forcing to models with both zonally symmetric and asymmetric backgrounds, the role of the background zonal asymmetry on MJO–SSW teleconnection can be isolated from that of asymmetry in the MJO forcing. The effect of the zonal asymmetry (restriction to a zonal window) of the MJO forcing can be diagnosed by comparing model experiments with realistic background forced with both circumglobal and longitudinally restricted MJO forcing. Since the MJO is projected to expand to a broader longitudinal range in a warmer climate (Chang et al. 2015), it is important to better understand the effects of the longitudinal location and extent of MJO forcing.

### c. Calculation of refractory index

The refractory index is calculated as follows (Vallis 2006):

$$n^2 = \left(\frac{Q_y}{U} - \frac{f^2}{4N^2H^2}\right) \times (a \cos\theta)^2, \\ Q_y = \beta - \frac{1}{a^2} \frac{\partial}{\partial\theta} \left(\frac{1}{\cos\theta} \frac{\partial U \cos\theta}{\partial\theta}\right) - f^2 \frac{1}{\rho} \frac{\partial}{\partial z} \left(\frac{\rho}{N^2} \frac{\partial U}{\partial z}\right), \quad (2)$$

where  $Q_y$  is the meridional gradient of the zonal-mean, time-mean potential vorticity,  $N^2$  is the Brunt–Väisälä frequency,  $H = RT/g$ ,  $f$  is the Coriolis parameter, and  $\beta$  is the meridional derivative of  $f$ .

We note that the refractory index in Eq. (2) is the square of the maximum wavenumber of stationary waves ( $\omega = 0$ ) allowed to propagate, while for transient waves, the climatological westerly wind speed  $U$  in Eq. (2) should be replaced by  $U - c_p$ , where  $c_p$  is the wave's phase speed. For  $k = 1$  waves propagating into the strong polar vortex ( $U \sim 60 \text{ m s}^{-1}$ ), the above definition may be applicable to all waves with frequency much lower than  $2\pi R_e \cos(60^\circ)/(60 \text{ m s}^{-1}) \sim 3.8 \text{ day}$ , where  $R_e$  is Earth's radius. Therefore, the definition in Eq. (2) is applicable to waves with periods longer than 38 days, within a 10% error, indicating more transmission in a weaker climatological  $U$ , a weaker stratification  $N^2$ , and a smaller  $U_{zz}$  and  $U_{yy}$ . For waves with periods between 3.8 and 38 days, the transmission will still change in the direction suggested by Eq. (2), but with a larger error.

### d. Diagnosing SSWs

Following Kim et al. (2017), two methods are used to diagnose SSWs in this work. The first identifies a SSW event when the zonal-mean zonal wind at  $60^\circ\text{N}$ , 10 mb is reversed to easterly, and thus captures only major SSW events. The second identifies an event when the zonal-mean zonal wind at  $60^\circ\text{N}$ , 10 mb, keeps decelerating at over  $5 \text{ m s}^{-1} \text{ day}^{-1}$  for at least 5 days, and therefore captures both major and minor SSW events. The SSW events are required to be at least 50 days apart in both approaches.

## 3. Results

The objective of this section is to present and understand the dependence of the SSW frequency on the MJO-forcing amplitude, and in particular to understand the role played by zonal asymmetries in both the background state and the MJO forcing. This dependence is therefore analyzed for both zonally symmetric and asymmetric backgrounds, as well as for varying zonal extents of the MJO-like forcing, from circumglobal forcing to forcing that is limited to a range of longitudes.

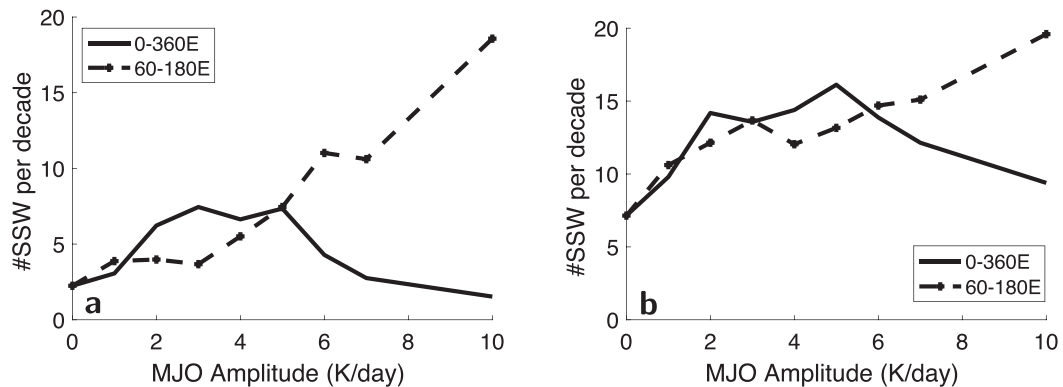


FIG. 1. The number of major SSW events per decade as a function of MJO amplitude. (a) The SSWs are identified based on wind reversal to include major SSWs only, and (b) are identified based on wind deceleration to include both major and minor SSWs (see section 2 for details). MJO forcing is applied around the globe (“circumblobal” cases) (solid line). MJO forcing is applied within the observed longitudinal window of 60°E–180° (dashed line).

Our main novel result in this paper is that the teleconnection between the MJO and the Arctic stratosphere, in particular the MJO effect on SSW events, critically depends on the zonal asymmetry of the background and on the longitudinal extent and location of the MJO forcing. We present the main results in section 3a. The mechanisms involving the role of the zonal asymmetry in the background state, the way it both affects the wave propagation and is affected by it, are analyzed in section 3b, while the role of the longitudinal location of the forcing itself is analyzed in section 3c.

#### a. Enhancement and suppression of SSW variability by MJO-like forcing

Figure 1 shows that when the MJO forcing is limited to a realistic longitude window of 60°E–180° [Eq. (1)], the SSW frequency increases with the MJO-forcing amplitude (dashed line), consistent with KT17. However, when the MJO forcing propagates uniformly around the globe (circumblobal forcing), the SSW frequency first increases and then decreases as the amplitude of this forcing increases (solid line). The two panels here correspond to the two SSW definitions used (see section 2 for details), and their similarity indicates that the results are robust to the details of the SSW definition.

Figure 2 shows the response of the climatological zonal-mean temperature  $T$  and zonal wind  $U$  to three representative amplitudes of the circumblobal MJO forcing (i.e., MJO2, MJO5, and MJO10 experiments). Shading by dots denotes 95% statistical significance based on the Student’s  $t$  test, using the number of years as a conservative estimate of the number of degree of freedom. The figure also shows 25-yr time series of the 60°N 10-mb zonal-mean zonal wind, as an SSW index, for these three forcing amplitudes, with SSW events

marked by small triangles along the time axis for both the CTRL (blue) and the MJO-forced (red) cases.

The MJO forcing has a very strong effect on the Arctic stratospheric climatology and variability: when forced by weak or medium-amplitude circumblobal MJO-like forcing (e.g., MJO2 and MJO5 in Figs. 2a,b), there are nearly 50% more SSWs than in the control run, and the Arctic stratosphere climatology warms up by over 3 K; while, when forced by even stronger forcing (e.g., MJO10 in Fig. 2c), there are only 3 SSW events in the shown 25 years, and an Arctic stratospheric cooling of more than 9 K occurs. The shown zonal-mean zonal wind responds consistently with the thermal wind balance, weakening in experiment MJO2 and MJO5, and strengthening in MJO10.

In the experiments with a medium circumblobal MJO-forcing amplitude (MJO5), SSW events tend to happen intermittently, with long gaps in between (there is only 1 SSW during years 25–35, while there are 11 during years 36–46), indicating that this case represents the transition between a regime with a higher frequency and a regime with a lower frequency of SSWs. As a reminder, the use of a circumblobal forcing is motivated both by the suggestions that the longitudinal extent of the MJO may widen in a warmer climate (Chang et al. 2015), and by the need to understand the role of zonal asymmetry in the background state alone. The response to MJO-like forcing that is restricted to a longitudinal window (experiments MJO[ $N$ ]Win, Table 1) is similar to the response to the weakly forced circumblobal experiments MJO2 and MJO5 (not shown).

The increase in SSW frequency and the polar stratospheric warming caused by MJO forcing was explained by KT17 via a combination of two mechanisms: first, the MJO-forced planetary waves directly propagate to the Arctic stratosphere and weaken the climatological polar

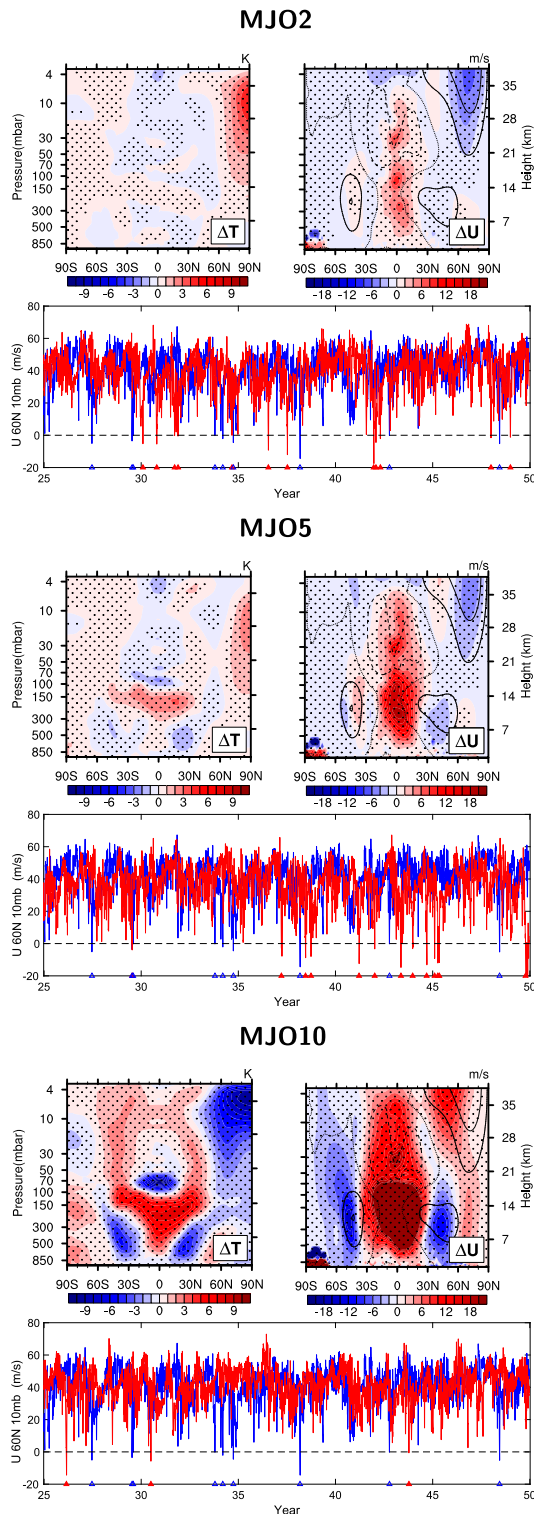


FIG. 2. Response to circumglobal MJO-like forcing with varying amplitudes in a model with a zonally asymmetric background, showing forced minus unforced model results: (from top to bottom) MJO2, MJO5, and MJO10, respectively. For each experiment, the top-left panel shows the zonally averaged climatological temperature response, the top-right panel shows zonally averaged zonal

night jet; second, there is a strengthening of the climatological stationary waves through a nonlinear interaction of the midlatitude jet with the MJO-forced transient waves. A teleconnection between the MJO and the polar cap temperature was noticed by Garfinkel et al. (2012), who explained it using yet another mechanism of a positive interference of MJO-forced waves and stationary waves in the North Pacific. We next build on the understanding of the above two mechanisms in order to explain why, under a stronger circumglobal MJO forcing ( $7$  and  $10 \text{ K day}^{-1}$ , Fig. 1), the occurrence of SSWs is suppressed and the polar cap cools.

In the strong circumglobal forcing runs (MJO7, MJO10), the MJO-forced waves do not affect the zonally averaged polar cap temperature although they do reach the Arctic stratosphere. This is seen by examining the zonally averaged response of the polar stratosphere to MJO forcing. Following Garfinkel et al. (2012), we show the composite of the averaged polar cap temperature ( $65^{\circ}$ – $90^{\circ}\text{N}$ ,  $10 \text{ mb}$ ) as function of the MJO phases and of the days since each phase, for experiments MJO2, MJO5, MJO10, and 2dMJO5 (Fig. 3). Although the MJO-forcing amplitude is smallest in MJO2 (Fig. 3a), the corresponding zonally averaged response in the Arctic stratosphere is the largest! The response to the MJO forcing in the MJO5 case (Fig. 3b) is similar to MJO2 although the MJO forcing is more than doubled. Further increasing the MJO-forcing amplitude (Fig. 3c, run MJO10), the zonally averaged MJO-composite temperature anomaly amplitude drops significantly.

Next, we need to understand if the lack of zonally averaged response of the polar cap to strong circumglobal MJO forcing is because MJO-forced waves do not propagate there, or because they do not affect the zonal mean. For this purpose, we diagnose the strength of the MJO-forced wave signal in the Arctic stratosphere: at each grid point, we calculate a temperature composite by MJO day (similarly to the composites based on the MJO phase, but at a higher temporal resolution), to calculate an amplitude, and we then take a zonal average of this amplitude, as shown in Fig. 4.

There are two important lessons from this figure. First, circumglobal MJO-forced waves do make it to the

←

wind response, and the bottom panel shows a time series of zonally averaged zonal velocity at  $60^{\circ}\text{N}$ ,  $10 \text{ mb}$ , for the unforced run (blue) and forced run (red). Dots denote 5% significance using the Student's  $t$  test. The climatological  $U$  wind from the unforced simulation is superimposed on the  $\Delta U$  panels, with solid contours corresponding to  $20$ ,  $40$ , and  $60 \text{ m s}^{-1}$ ; dashed contours correspond to  $-20$  and  $-40 \text{ m s}^{-1}$ ; and dotted contours correspond to the zero of the  $U$  wind.

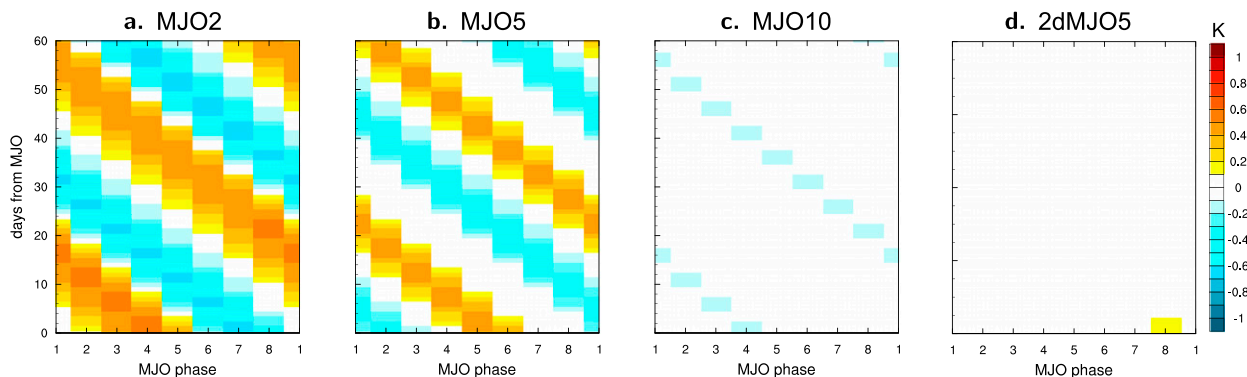


FIG. 3. Composite of polar cap temperature ( $65^{\circ}$ – $90^{\circ}$ N, 10 mb) as function of the MJO phase (horizontal axis) and days since each phase (vertical), following Garfinkel et al. (2012). Results are shown for (a) MJO2, (b) MJO5, (c) MJO10, and (d) 2dMJO5.

Arctic stratosphere in the strongly forced case MJO10, even though this is not expressed in the zonally averaged response shown in Fig. 3. Second, the amplitude of this Arctic response does not increase linearly with the MJO amplitude, but in fact reaches a maximum and then decreases: going from MJO2 to MJO5 (from MJO5 to MJO10), the forcing strength is increased by a factor of 2.5 (factor of 2), while the RMS of the MJO-forced variability in the Arctic stratosphere is only enhanced by 50% (reduced by 20%).

#### b. How background zonal asymmetries affect the MJO–SSW teleconnection

This subsection proceeds as follows. We first show in section 3b(1) that the Arctic temperature response to strong MJO-like forcing is similar to that in the runs with a zonally averaged background state, because the zonal asymmetry of the background state is weakened in the strongly forced runs (e.g., MJO10) through an interaction between the MJO-forced waves and the

background flow. Section 3b(2) then shows that this zonal asymmetry in the background state enables the propagation of MJO-forced waves to the polar cap, and therefore determines their ability to influence the zonally averaged temperature. Next, section 3b(3) shows that the weakening of midlatitude jet gives rise to the weakening of waves generated in the midlatitudes, especially stationary waves. Finally, in section 3b(4), we show that the transmission of large-scale upward-propagating waves (including both MJO-forced waves and waves generated in the midlatitudes) from the lower subpolar stratosphere to the upper polar stratosphere decreases, because of a reduction in the refractory index.

#### 1) RESPONSE TO STRONG CIRCUMGLOBAL MJO-LIKE FORCING, AND RESPONSE WITH A ZONALLY SYMMETRIC BACKGROUND

To isolate the role played by the background zonal asymmetry, we first run idealized experiments with and without such asymmetry, and force them using a

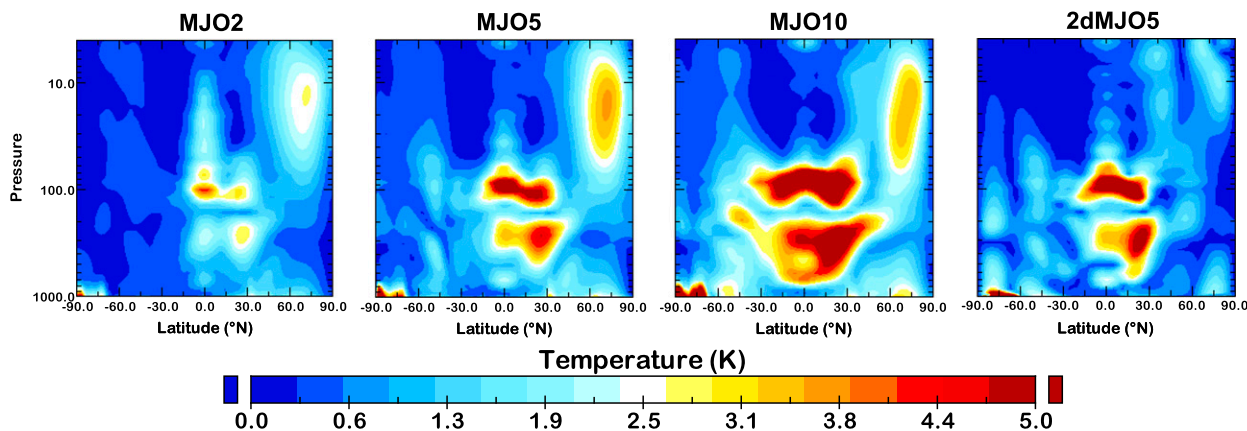


FIG. 4. The zonally averaged amplitude of temperature anomalies due to MJO forcing, as function of latitude and pressure (see text for details): (from left to right) MJO2, MJO5, MJO10, and 2dMJO. Note that the experiment with medium forcing amplitude,  $5 \text{ K day}^{-1}$ , rather than the strongest-forced one, shows the largest amplitude response in the Arctic stratosphere.

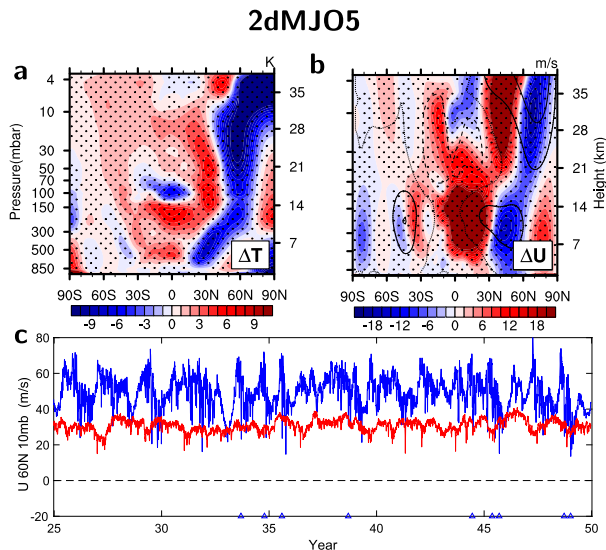


FIG. 5. As in Fig. 2, but showing the response of temperature,  $U$  wind, and SSW time series, in the experiment with zonally symmetric background, 2dMJO5. Because the unforced control experiment of this model does not show major SSW events, we mark minor ones, as defined in Fig. 1. Note that no such minor events occur in the forced run.

circumglobal MJO forcing at a range of amplitudes. Since the response in the zonally symmetric experiments does not change qualitatively with the MJO amplitude, we show only 2dMJO5 here as an example. As shown in Fig. 5, the Arctic climatological temperature cooling response is quite similar in MJO10 and 2dMJO5, and so are the tropospheric changes to the zonally averaged zonal velocities in the Northern Hemisphere, while the zonal-mean zonal wind response is different in the NH stratosphere and in the Southern Hemisphere. While no major SSW events happen in the zonally symmetric simulations, the number of minor SSW events reduces from 19 per 50 years in the control case, to none in the forced case, similar to the MJO10 case (Fig. 2c; minor events are diagnosed as in Fig. 1b). Also similar to MJO10, the polar cap temperature rarely varies with MJO phases in 2dMJO5 (Fig. 3d), and the standard deviation of temperature composite based on MJO days (Fig. 4d) is also very small in the Arctic stratosphere.

The reason for this similarity of the Arctic temperature response in the zonally averaged background case 2dMJO5 and the strongly forced case MJO10, is that the background zonal asymmetry in MJO10 is weakened by the interaction between the MJO forced waves and the mean flow. This makes the background of the MJO10 experiment more similar to that of 2dMJO5. To see the change of the background zonal asymmetry, we project the meteorological fields onto large-scale wavenumber-1

structure here, and we also evaluate the EP flux associated with the stationary waves in a later subsection. In the midlatitudes (averaged between 250 and 350 mb,  $45^{\circ}$ – $55^{\circ}$ N), adding a strong ( $10 \text{ K day}^{-1}$ ) MJO forcing leads to a reduction in the wavenumber-1 amplitude of  $T$ ,  $U$ , and  $V$ , from 1.80 to  $1.12 \text{ K}$ , from  $8.43$  to  $4.21 \text{ m s}^{-1}$ , and from  $1.46$  to  $1.40 \text{ m s}^{-1}$ , respectively. Consistently, the stationary wave EP flux also decreases, as discussed in section 3b(3) as part of the discussion of a second suppression mechanism.

The vanishing of the zonally averaged response in the zonally symmetric experiment (2dMJO5, Fig. 3d) is expected: without zonal asymmetry in either the background or the MJO-forcing amplitude, all MJO phases and all longitudes are equivalent. Thus, an MJO-induced polar stratospheric warming at a given longitude is accompanied by cooling at a longitude that is  $180^{\circ}$  away, such that the zonally averaged temperature anomaly correlated with the MJO vanishes. This longitudinal cancellation may explain why the reduction in the zonally averaged amplitude from MJO5 to MJO10 shown in Figs. 3b,c is much more significant compared to the amplitude of the waves actually reaching the Arctic (Figs. 4b,c): the strongly forced waves create a more zonally symmetric background, propagate through it, and their zonally symmetric signature on the Arctic cap is accordingly smaller.

## 2) EFFECTS OF THE ZONAL BACKGROUND ASYMMETRY ON THE TRANSMISSION OF CIRCUMGLOBAL MJO-FORCED WAVES THROUGH THE MIDLATITUDE JET

To propagate into the midlatitude lower stratosphere, the MJO-forced waves need to first propagate past the tropospheric jet. The zonal asymmetry of the background state near the jet exit, where  $-U_x$  is larger, may strengthen the transient waves via an energy transfer from the mean flow via the term  $(\overline{u'^2} - \overline{v'^2})U_x$  in the kinetic energy equation (Simmons et al. 1983), and lead to accumulation of wave activity due to a convergence of group velocity induced by the convergence of the mean flow (Webster and Chang 1988). This is consistent with the result in KT17 and Garfinkel et al. (2012, 2014) that poleward propagation of MJO-forced waves is only possible during specific MJO phases (i.e., when the maximum heating rate is at the right longitudes).

As shown in the last subsection, when removing the background zonal asymmetries (experiment 2dMJO5), the amplitude of the MJO-forced waves in the Arctic stratosphere is very weak (Fig. 4d), indicating they can reach the Arctic only in the presence of a midlatitude zonal asymmetry. The MJO-related signal in MJO10

weakens poleward of 45°N, much more than it weakens in MJO5 (Fig. 4b). This suggests that a weaker transmission of the MJO-forced waves in MJO10 is through the midlatitude upper troposphere. To quantify this effect, we define a transmission coefficient  $\gamma$  as

$$\gamma = \sqrt{\frac{\int_{45^{\circ}\text{N}}^{65^{\circ}\text{N}} \text{EP}_{z,\text{MJO}}|_{100\text{mb}} dy}{\int_{100\text{mb}}^{400\text{mb}} \text{EP}_{y,\text{MJO}}|_{25^{\circ}\text{N}} dp}}, \quad (3)$$

where  $(\text{EP}_{y,\text{MJO}}, \text{EP}_{z,\text{MJO}})$  are the MJO-associated EP fluxes, calculated based on  $u'$ ,  $v'$ , and  $T'$  that are filtered at a 40-day period. We picked the range of the above integrals such that they are close to the midlatitude jet exit region we are interested in, and also reflect the transmission from the subtropical troposphere to the Arctic stratosphere. To quantify the strongest jet convergence due to  $U$ , we take average of the climatological zonal wind component between 100 and 300 mb, and pick the maximum zonal convergence,  $-U_x$ , between 35° and 55°N, denoting this strongest convergence as  $C_U$ .

We first check the correlation between the transmission coefficient  $\gamma$  and the strongest jet convergence defined above for the experiments MJO1–MJO10, and show a scatterplot of  $\gamma$  versus  $C_U$  in the unfilled circles in Fig. 6. Their correlation is high, 0.81, and is not sensitive to the integral intervals in Eq. (3) (e.g., changing the integral latitudinal interval in the nominator to 35°–55°N or 45°–75°N also yields  $r = 0.8$ ). A similar transmission enhancement by the background zonal asymmetry was also noticed by Blackmon et al. (1987) and Ting and Sardeshmukh (1993) in the context of studying the response to tropical perturbations in general, and by Lin and Brunet (2018), Goss and Feldstein (2015), Bladé and Hartmann (1995), and O'Brien et al. (1994) in the context of the MJO.

Then, to validate the effect of the zonal asymmetry on the transmission of MJO-forced waves, we run a series of experiments with  $2\text{K day}^{-1}$  circumglobal MJO forcing, but with different degrees of background zonal asymmetry, where we modify the amplitude of the asymmetric component of the background-maintaining forcing, both with and without topography (see section 2). These experiments are represented in Fig. 6 with filled circles labeled by the experiment names ( $[S]\%$  and  $[S]\% + \text{topo}$ , see Table 1). The transmission of MJO-forced waves is positively correlated with the maximum midlatitude jet convergence in these experiments, both within the group of experiments with topography and within the experiments with flat topography. This confirms that stronger background zonal asymmetry does improve the transmission.

The specific measure of midlatitude wind convergence used here to quantify the zonal asymmetry is motivated

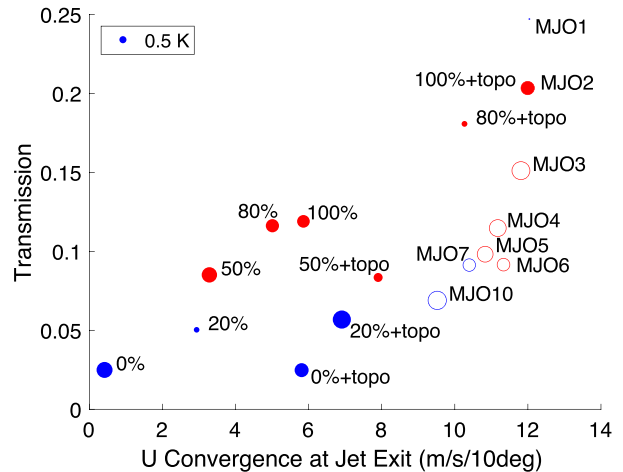


FIG. 6. The dependence of the transmission of MJO-forced waves toward the Arctic stratosphere on the background state, where the transmission coefficient is defined in Eq. (3), and the background zonal asymmetry is measured by the strongest jet convergence along the zonal circle between 35° and 55°N, averaged over 100–300 mb (see text for details). Each point corresponds to a model run and is labeled using the experiment name (Table 1). Filled dots correspond to the experiments with modified zonal asymmetry ( $[S]\%$  and  $[S]\% + \text{topo}$ ), forced by  $2\text{K day}^{-1}$  circumglobal MJO forcing, and unfilled dots correspond to the experiments with full asymmetry, but different (circumglobal) MJO amplitudes. Note that the MJO2 and 100% + topo experiments are equivalent. The size of dots denotes the amplitude of the warming (red) or cooling (blue) in the Arctic stratosphere between 20 and 30 mb, 70° and 90°N, compared with the corresponding unforced simulations.

by Simmons et al. (1983), and further research is needed to understand which specific features of the jet improve the transmission and what is the corresponding mechanism. Using an alternative measure of the background zonal asymmetry, based on the stationary  $\text{EP}_z$ , also leads to a high correlation coefficient, of 0.92.

Finally, we investigate whether the transmission rate of MJO-forced waves affects the response in the Arctic stratosphere, by showing the Arctic stratospheric warming (forced minus unforced, 20–40 mb, 70°–90°N). In Fig. 6, the size of the dots denotes the warming/cooling amplitude, with blue corresponding to cooling and red corresponding to warming. With a transmission rate greater than 0.1, the Arctic stratosphere is generally warmed up, and vice versa. The figure also shows that experiments with the same transmission rate of the MJO-forced waves lead to a different responses in the Arctic stratosphere. This is because 1) the unforced climatologies are very different in these experiments, and 2) there are other mechanisms involved in the MJO–Arctic teleconnection, as described in the following section. As a motivation for examining the effect on the generation of waves in the midlatitudes in the

next section, note that even if the transmission of MJO waves is completely blocked by the midlatitude jet, one would merely expect weaker Arctic warming due to the MJO-forced waves, but not a cooling as we observe in some of these experiments.

### 3) SUPPRESSION OF MIDLATITUDE-GENERATED WAVES BY THE MJO-LIKE FORCING

We find that a suppression of the midlatitude-generated waves is one of the mechanisms that leads to a cooling of the Arctic stratosphere by MJO forcing. We first consider the temperature budget for the region  $75^{\circ}$ – $85^{\circ}$ N and 10–40 mb (calculated as in KT17, not shown), and the warming (cooling) of the Arctic cap in response to weak (strong) MJO forcing, and find it to be driven by an increase (decrease) of the total vertical EP flux. We further decompose the total  $EP_z$  between  $50^{\circ}$  and  $90^{\circ}$ N at 100 mb into three components (Fig. 7): 1) the MJO-related transient waves in red, 2) the stationary waves in green, and 3) other transient waves, defined as the transient waves that are not related to the MJO, in blue. To evaluate the MJO-related transient waves, we first filtered the daily  $U$ ,  $V$ , and  $T$  to find the signal with a 40-day period (the MJO forcing period), and with zonal wavenumbers  $k = 1, 2$ . These filtered fields are then used to calculate  $u'v'$  and  $v'T'$  used in the EP flux formula, where primes in this case denote deviation from time mean. The EP fluxes due to stationary waves are calculated using the deviation of the climatological  $U$ ,  $V$ , and  $T$  from their zonal mean. The third component is the residual EP flux excluding the first two components, representing transient waves not directly associated with the MJO forcing. The transmission of MJO-forced waves was shown in section 3b(2) to decrease as the zonal asymmetry weakens because of stronger MJO forcing, although the *total* transmitted EP flux monotonically increases with the MJO-forcing amplitude. The stationary wave component and the non-MJO-related transient wave component change in the opposite directions, with an 83% reduction in the stationary wave component and a 32% enhancement in the non-MJO-related transient wave component.

Figure 8 shows the forced minus unforced EP flux vectors and EP flux divergence, for the three components described above, and for experiments MJO10 and 2dMJO5. In MJO10, the MJO-related transient wave EP flux (top panels) can travel to the Arctic region in MJO10 and weaken the polar night jet there, while, in 2dMJO5, these waves stop propagating northward before the midlatitudes. This is consistent with section 3b(2) where it was shown that the MJO-forced waves can travel only in the presence of an asymmetry in the background jets. The total response of the stationary

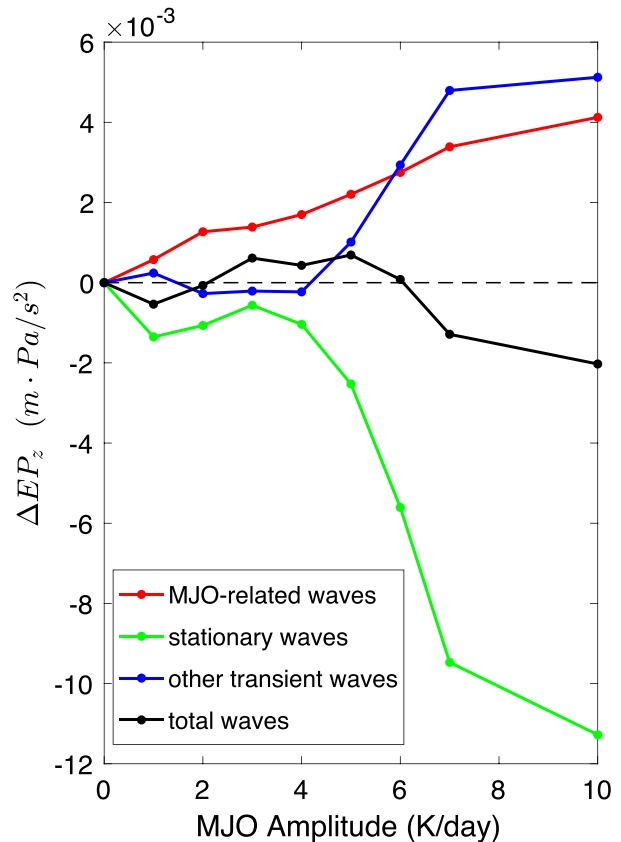


FIG. 7. The role of different waves in the SSW enhancement and suppression mechanisms. The response (forced minus unforced amplitude) of upward EP flux at the Arctic tropopause ( $50^{\circ}$ – $90^{\circ}$ N, 100 mb) due to waves associated with MJO-forcing (red), stationary waves (green), waves excluding MJO-forced signal and the stationary waves (blue), and all waves (black).

waves (middle panels) and the non-MJO-related transient waves (bottom panels) acts to strengthen the jet in both experiments MJO10 and 2dMJO5.

In MJO10, the stationary  $EP_z$  in the Arctic stratosphere is weakened significantly while the non-MJO-related transient  $EP_z$  is somewhat strengthened, as are the transmitted MJO-related waves. On one hand, the stationary wave activity weakens, because of the weakened westerly jet that flows over NH topography, as shown in Fig. 2c [see Fig. 6.1 in Held (1983), for the resonance jet speed], due to the equatorward eddy momentum transport associated with the MJO-forced waves. The top panels of Fig. 8 show that the MJO-related EP flux forced at the equator is absorbed in the midlatitudes, decelerating the jets there. We note that these MJO-forced waves also force a superrotation in the upper troposphere, for forcing amplitudes larger than  $2 \text{ K day}^{-1}$  in the circumglobal experiment, and for amplitudes larger than  $3\text{--}4 \text{ K day}^{-1}$  in the longitudinally restricted forcing. The mechanism of the stationary

wave response, involving the effect of transient waves on the background zonal asymmetry, requires further work beyond the scope of this study.

On the other hand, the upward EP flux associated with the non MJO-related transient waves strengthens, emanating from  $70^\circ$  to  $90^\circ\text{E}$ , and the strengthening is consistent with the enhanced Eady growth rate in that region (not shown). The Eady growth rate likely only affects synoptic eddies at a time scale of a few days and zonal wavenumbers around  $k = 4 - 6$ , incapable of propagating into the Arctic stratosphere. However, nonlinear interaction between synoptic-scale waves and the corresponding inverse cascade may lead to enhanced planetary-scale wave activity at  $k = 1, 2$  that can propagate to the Arctic stratosphere. We filtered the meteorological fields by a 1–15-day period to calculate the EP flux associated with transient motions forced by synoptic eddies, and find it to also be enhanced in the Arctic stratosphere (not shown, we also note that when filtering for 1–7 days, there is no EP flux enhancement in the stratosphere).

In the zonally averaged background experiment 2dMJO5, the stationary wave contribution is, by definition, zero, with or without MJO forcing, thus the corresponding panel in Fig. 8 is left blank. In 2dMJO5, the response of the non-MJO-related transient waves alone resembles the total response of stationary and other transient waves in MJO10 (not shown).

Precisely how and why the amplitude of midlatitude stationary waves changes under MJO forcing requires further study. We may have ignored some potential links by treating the stationary component and the non-MJO-related transient component separately, especially given the cancellation between them (Figs. 7, 8). We note that the response of total EP in MJO10 is fairly similar to 2dMJO5, even if there is no stationary wave and corresponding feedbacks in 2dMJO5 at all. In addition, the constructive interference of the MJO-forced waves with the climatological stationary waves (Garfinkel et al. 2014, 2012; Schwartz and Garfinkel 2017) may also play a role in changing the SSW frequency by strengthening  $\text{EP}_z$  during certain times and weakening  $\text{EP}_z$  during other times, even if it cannot change the time-averaged  $\text{EP}_z$ . See also Ineson and Scaife (2009) and Kim et al. (2014) for a related analysis of constructive/destructive interference of the climatological waves with perturbations forced by El Niño and by sea ice anomalies.

#### 4) REDIRECTION OF UPWARD-PROPAGATING WAVES AWAY FROM THE ARCTIC STRATOSPHERE

Once the MJO-forced waves make it past the jet exit region into the lower stratosphere at midlatitudes, they

need to continue to the high-latitude upper stratosphere in order to affect the Arctic cap. Figure 4 shows that MJO10 has a smaller-amplitude MJO-related variability in the high-latitude stratosphere than MJO5, although its midlatitude tropospheric variability is stronger. This indicates that upward propagation toward the Arctic stratosphere is suppressed in MJO10. This propagation is affected by the decreased refractory index in the Arctic stratosphere (Fig. 9b). Consistent with the similarity of the Arctic stratospheric cooling response in 2dMJO5 and MJO10 [section 3b(1)], both experiments show decreasing of refractory index over the Arctic stratosphere and increasing in the midlatitude stratosphere. The reduction of refractory index in the high-latitude stratosphere is due to the reduced  $U_{zz}$  in 2dMJO5, while in MJO10 it is caused by the combined effects of decreased  $U_{zz}$  and  $U_{yy}$  and a strengthened  $U$ . However, we note here that the refractory index response in MJO10 (Fig. 9b) is not as significant as in 2dMJO5 (Fig. 9c), adding some doubt regarding the role played by this mechanism in the reduction of Arctic stratospheric  $\text{EP}_z$  in MJO10.

To see to what extent the refractory index change may affect planetary wave transmission, we define another transmission factor, for upward propagation of MJO-forced waves from the lower stratosphere at mid-latitudes, to the upper stratosphere at higher latitudes, focusing on the region with reduced refractory index in Fig. 9b. The factor is calculated as the ratio of the MJO-forced temperature anomaly amplitude (as shown in Fig. 4) averaged over 7–15 mb,  $70^\circ$ – $90^\circ\text{N}$ , to that averaged over 50–70 mb,  $55^\circ$ – $65^\circ\text{N}$ . Figure 9a is a scatterplot of this transmission coefficient versus the Arctic stratospheric refractory index [Eq. (2)], in all the forced experiments with a realistic zonally asymmetric background. The figure shows a strong correlation between these two measures, indicating that the reduction in refractory index in the Arctic stratosphere explains the reduced transmission of MJO-forced waves in the strongly forced cases.

#### c. Role of the zonal location of the MJO forcing

The above analysis was based on circumglobal MJO-like forcing, and we now move one more step toward realism and explore the role of longitudinally restricted MJO-forcing, which in current climate occurs within  $60^\circ\text{E}$ – $180^\circ$ . As shown in Fig. 1, this longitudinal extent does make a difference in the Arctic stratospheric response to MJO amplitudes: the SSW frequency monotonically increases with MJO amplitudes for longitudinally restricted forcing, rather than being suppressed under strong circumglobal MJO forcing. We ran three experiments with MJO forcing restricted

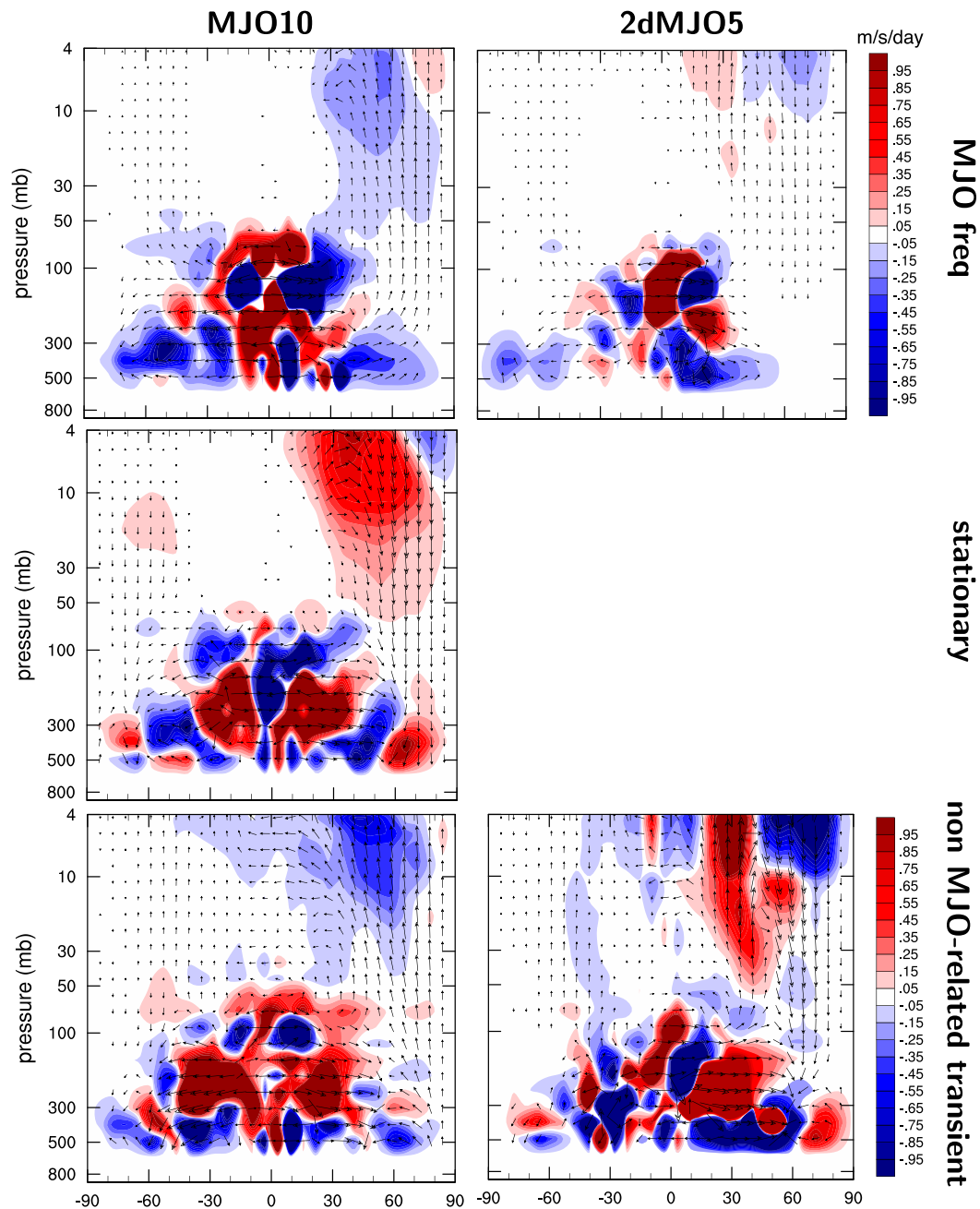


FIG. 8. The EP flux (arrows) and its divergence (shading), showing the response to MJO forcing (forced minus unforced climatologies). (top) MJO-related waves, (middle) the stationary waves, and (bottom) non-MJO-related transient waves (defined in text), and (left) for the strongly forced experiment MJO10 and (right) the experiment with zonally symmetric background, 2dMJO5. The arrow lengths are proportional to the 1/3 power of the EP flux vector length, to allow clearly displaying a wide range of EP amplitudes.

to different longitudinal bands (MJO5Win60–180, MJO5Win180–300, MJO5Win300–60), and with a realistic asymmetric background, to investigate whether the location of the MJO forcing matters.

The responses of the zonally averaged climatological temperature are plotted in Fig. 10. When the forcing is at

60°E–180° (Fig. 10a), where the observed MJO occurs, the Arctic stratospheric warming is as high as 5 K; when the forcing is at 180°–300°E (Fig. 10b), the warming turns into a cooling of 3 K; and when moving the forcing is at 300°–60°E (Fig. 10c), the warming is weakened to less than 2 K. The SSW frequency also changes accordingly,

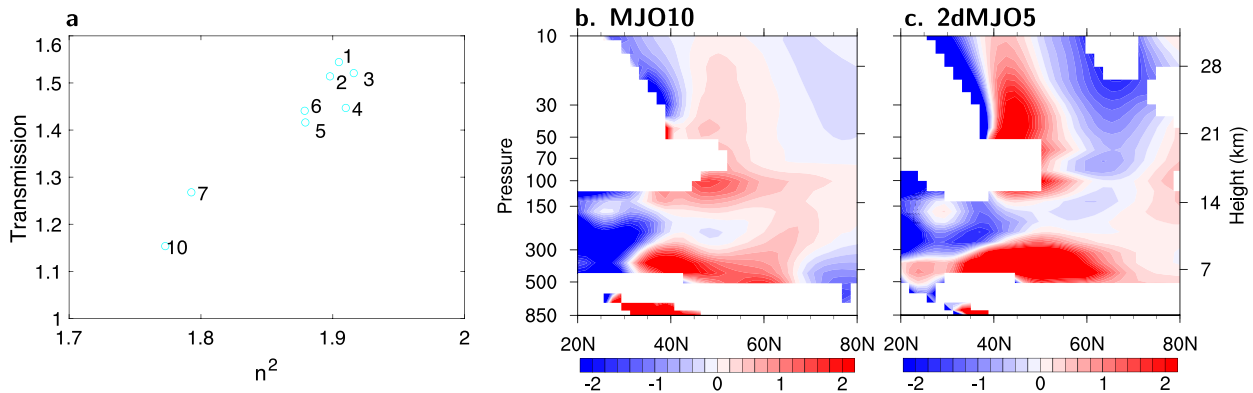


FIG. 9. (a) A scatterplot of the transmission rate from the lower stratosphere to the middle stratosphere in the Arctic, as a function of the Rossby wave refractive index. (b),(c) Response of the Rossby wave refractive index to MJO-like forcing, showing forced minus unforced fields for MJO10 and 2dMJO5. The refractory index [ $n^2$ , Eq. (2)], is in units of the number of full wavelength along the zonal circle. Missing values in refractory index indicate  $n^2 < 0$  in either the control or forced experiments.

increasing from 3.8 to 7.2 decade<sup>-1</sup> in the realistic window of MJO5Win60–180, decreasing to 2.0 decade<sup>-1</sup> in MJO5Win180–300 and decreasing to 3.2 decade<sup>-1</sup> in MJO5Win300–60. This dominant effect of the longitudinal location of the forcing is consistent with previous findings that showed the longitudinal location of equatorial forcing to affect poleward propagation in idealized baroclinic (Jin and Hoskins 1995) and barotropic (Naoe and Matsuda 1998) models.

The three suppression mechanisms in section 3b may provide some insights into the Arctic stratospheric cooling and the suppression of SSWs in MJO5Win180–300, representing MJO forcing just east of the observed window. We hypothesize that the MJO forcing in this window changes the jet to be more zonally symmetric and therefore reduces the transmission of the MJO-forced waves as well as reduces stationary waves forced at the mid-latitudes. The detailed analysis of this hypothesis is outside the scope of the present paper and will be the subject of a future work.

#### 4. Conclusions

We analyzed the role of zonal asymmetry in the teleconnection between the Madden–Julian oscillation (MJO) and sudden stratospheric warming (SSW) events, for a range of MJO amplitudes and longitudinal configurations, motivated by the strengthening of the MJO amplitude (e.g., Slingo et al. 1999; Hendon et al. 1999; Jones and Carvalho 2006; Caballero and Huber 2010; Oliver and Thompson 2012; Schubert et al. 2013; Arnold et al. 2013, 2014) and by the wider MJO longitudinal extension (Chang et al. 2015) predicted in a warmer climate. We applied idealized MJO-like forcing, either restricted to a certain longitudinal window (corresponding to the longitudinal-restricted MJO in the current climate),

or propagating uniformly around the equator (circumglobal, motivated by the need to examine the role of zonal asymmetry in the background state alone). The background state of the dry-core model used, was set to either a January climatology, or to its zonal average. These experiments allowed us to analyze the role of the zonal asymmetry in both the forcing and the background state.

As the MJO-forcing amplitude is increased, the Arctic stratosphere climatology, and the frequency of SSW events, respond to the MJO-like forcing depending on the zonal asymmetry of both the background and the forcing. When the forcing is limited to the longitude band along the equator occupied by the observed MJO and the background state is realistic, the Arctic warms and the SSW frequency increases with the MJO amplitude. When the forcing is circumglobal, even in the presence of a realistically zonally asymmetric background, increasing the MJO amplitude leads first to an enhancement of the SSW frequency but then to its suppression. Making the problem even more zonally symmetric, by removing zonal asymmetry from the background and using circumglobal forcing, the MJO forcing can only suppress any SSW variability and lead to a cooling of the Arctic stratospheric climatology. Finally, when the background is realistically zonally asymmetric and the MJO-like forcing is limited to a longitudewindow, the location of this forcing can still make a significant difference: the MJO forcing enhances the SSW frequency and leads to warming of the stratosphere only if it is placed in the Indo-Pacific section.

The SSW frequency enhancement mechanism was shown by Kang and Tziperman (2017) to involve two effects: first, the direct propagation of the MJO-forced transient waves, and second, the enhancement of the climatological stationary waves caused by a nonlinear

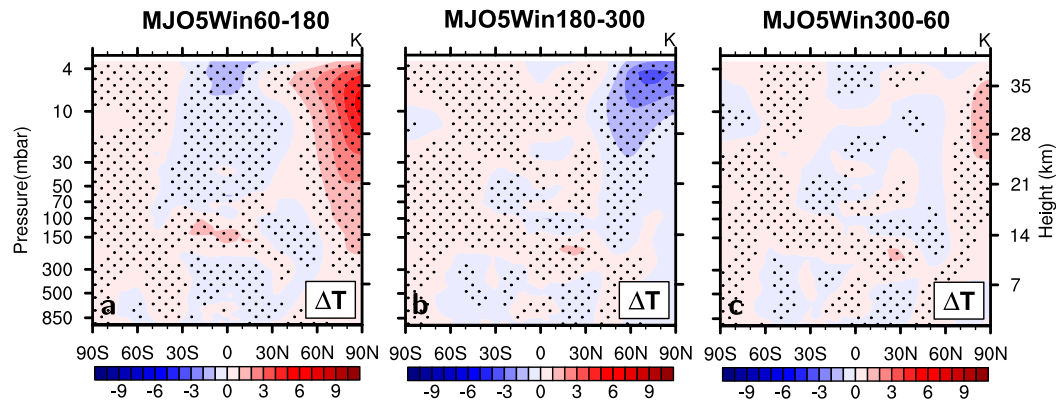


FIG. 10. Response of the zonally averaged temperature in a zonally asymmetric model to longitudinally restricted MJO-like forcing when the forcing is applied at (a) 60°E–180°, (b) 180°–300°E, and (c) 300°–60°E. When the forcing is applied in the window corresponding to the observed MJO [as in (a)], the warming response is maximal.

wave–mean flow interaction between the MJO-forced waves and the midlatitude jet. Garfinkel et al. (2014, 2012) and Schwartz and Garfinkel (2017) also noted an effect of the MJO on the polar cap temperature, and a redistribution of the SSW events according to MJO phases, although they did not consider the response of the SSW frequency or the response to a strengthening MJO in a warming scenario. These authors suggested an alternative MJO–SSW teleconnection mechanism, involving a constructive interference of the MJO-forced waves and the climatological stationary waves. We showed here that the MJO-forced waves can propagate past the midlatitude jet because of its zonal asymmetries, consistent with previous studies that emphasized the role of the zonal convergence in the jet-exit region (Simmons et al. 1983; Branstator 1985; Webster and Chang 1988; Naoe et al. 1997; Hoskins and Jin 1991; Bao and Hartmann 2014).

The mechanism by which MJO-like forcing can suppress the SSW variability, either when the forcing is circumglobal, or when it is longitudinally restricted to other than the observed longitudinal band, involves three factors:

- The midlatitude background zonal asymmetry decreases with stronger MJO forcing, weakening the poleward transmission of MJO-forced waves.
- The MJO-forced waves absorbed in the midlatitudes decelerate the midlatitude jet, weaken the upward propagating stationary wave generated in the midlatitude, although this effect is partially compensated for by the enhancement of transient waves generated in the high latitudes, making the Arctic stratosphere colder and more stable.
- The MJO-driven waves lead to a modification of the jet speed and shear in the lower stratosphere and therefore reduces the Arctic refractory index, which may refract upward-propagating waves away from the

Arctic stratosphere and therefore enhance the cooling of the Arctic stratosphere.

All three effects reduce the wave activity and therefore eddy heat flux arriving to the stratospheric Arctic cap, cool and stabilize the Arctic stratosphere, and reduce the frequency of SSW events.

It should be noted that the analysis here is based on a highly idealized model, where the MJO is not explicitly simulated and moisture feedbacks are ignored, among other simplifications. While this allows a deeper understanding of the results, a verification using more complete GCMs is required. We also note that, because of the relative low model top being used (3 mb), the SSW simulated in the idealized model may be not realistic. The strongest MJO forcing used here is  $10 \text{ K day}^{-1}$ . This value is significantly larger than current values of  $2\text{--}4 \text{ K day}^{-1}$ , but may be possible in a  $4 \times \text{CO}_2$  (Arnold et al. 2015) or even more extreme warming scenarios. At a  $10 \text{ K day}^{-1}$  forcing amplitude, the mean atmospheric state is significantly modified by the forcing (Fig. 2c). We discussed how these mean state changes affect the teleconnection mechanism, yet it is useful to keep in mind that the mean state is very different from the present-day atmosphere in this case, making it likely an unrealistic scenario, even if useful for understanding purposes.

This work suggests that in order to predict changes in the MJO–SSW teleconnection in a warmer climate, it is important to predict, in addition to the MJO amplitude, also its zonal extent and the asymmetry of the background midlatitude state. All three factors can affect the teleconnection and therefore have implications on downward propagation, including the Arctic Oscillation, midlatitude blocking systems, and extreme weather events (e.g., Baldwin and Dunkerton 1999; Gerber and Polvani 2009; Thompson et al. 2002; Cohen et al. 2007; Kolstad et al. 2010).

*Acknowledgments.* We thank three anonymous reviewers for their helpful feedback. This work was supported by the NSF P2C2 program, Grant OCE-1602864, and by funding from the Harvard Global Institute and Harvard Climate Solutions fund. ET thanks the Weizmann Institute for its hospitality during parts of this work. We would like to acknowledge high-performance computing support from Yellowstone provided by NCAR's Computational and Information Systems Laboratory, sponsored by the National Science Foundation.

## REFERENCES

- Arnold, N., Z. Kuang, and E. Tziperman, 2013: Enhanced MJO-like variability at high SST. *J. Climate*, **26**, 988–1001, <https://doi.org/10.1175/JCLI-D-12-00272.1>.
- , M. Branson, M. A. Burt, D. S. Abbot, Z. Kuang, D. A. Randall, and E. Tziperman, 2014: Effects of explicit atmospheric convection at high CO<sub>2</sub>. *Proc. Natl. Acad. Sci. USA*, **111**, 10 943–10 948, <https://doi.org/10.1073/pnas.1407175111>.
- , —, Z. Kuang, D. A. Randall, and E. Tziperman, 2015: MJO intensification with warming in the Super-Parameterized CESM. *J. Climate*, **28**, 2706–2724, <https://doi.org/10.1175/JCLI-D-14-00494.1>.
- Baldwin, M. P., and T. J. Dunkerton, 1999: Propagation of the Arctic Oscillation from the stratosphere to the troposphere. *J. Geophys. Res.*, **104**, 30 937–30 946, <https://doi.org/10.1029/1999JD900445>.
- Bancalá, S., K. Krüger, and M. Giorgetta, 2012: The preconditioning of major sudden stratospheric warmings. *J. Geophys. Res.*, **117**, D04101, <https://doi.org/10.1029/2011JD016769>.
- Bao, M., and D. L. Hartmann, 2014: The response to MJO-like forcing in a nonlinear shallow-water model. *Geophys. Res. Lett.*, **41**, 1322–1328, <https://doi.org/10.1002/2013GL057683>.
- Bell, C. J., L. J. Gray, and J. Kettleborough, 2010: Changes in Northern Hemisphere stratospheric variability under increased CO<sub>2</sub> concentrations. *Quart. J. Roy. Meteor. Soc.*, **136**, 1181–1190, <https://doi.org/10.1002/qj.633>.
- Blackmon, M. L., G. W. Branstator, G. T. Bates, and J. E. Geisler, 1987: An analysis of equatorial Pacific sea surface temperature anomaly experiments in general circulation models with and without mountains. *J. Atmos. Sci.*, **44**, 1828–1844, [https://doi.org/10.1175/1520-0469\(1987\)044<1828:AAOEPS>2.0.CO;2](https://doi.org/10.1175/1520-0469(1987)044<1828:AAOEPS>2.0.CO;2).
- Bladé, I., and D. L. Hartmann, 1995: The linear and nonlinear extratropical response of the atmosphere to tropical intraseasonal heating. *J. Atmos. Sci.*, **52**, 4448–4471, [https://doi.org/10.1175/1520-0469\(1995\)052<4448:TLANER>2.0.CO;2](https://doi.org/10.1175/1520-0469(1995)052<4448:TLANER>2.0.CO;2).
- Branstator, G., 1985: Analysis of general circulation model sea-surface temperature anomaly simulations using a linear model. Part I: Forced solutions. *J. Atmos. Sci.*, **42**, 2225–2241, [https://doi.org/10.1175/1520-0469\(1985\)042<2225:AOGCMS>2.0.CO;2](https://doi.org/10.1175/1520-0469(1985)042<2225:AOGCMS>2.0.CO;2).
- Butchart, N., J. Austin, J. R. Knight, A. A. Scaife, and M. L. Gallani, 2000: The response of the stratospheric climate to projected changes in the concentrations of well-mixed greenhouse gases from 1992 to 2051. *J. Climate*, **13**, 2142–2159, [https://doi.org/10.1175/1520-0442\(2000\)013<2142:TROTSC>2.0.CO;2](https://doi.org/10.1175/1520-0442(2000)013<2142:TROTSC>2.0.CO;2).
- Caballero, R., and M. Huber, 2010: Spontaneous transition to superrotation in warm climates simulated by CAM3. *Geophys. Res. Lett.*, **37**, L11701, <https://doi.org/10.1029/2010GL043468>.
- Cassou, C., 2008: Intraseasonal interaction between the Madden-Julian Oscillation and the North Atlantic Oscillation. *Nature*, **455**, 523–527, <https://doi.org/10.1038/nature07286>.
- Chang, C. W. J., W. L. Tseng, H. H. Hsu, N. Keenlyside, and B. J. Tsuang, 2015: The Madden-Julian Oscillation in a warmer world. *Geophys. Res. Lett.*, **42**, 6034–6042, <https://doi.org/10.1002/2015GL065095>.
- Charlton-Perez, A. J., L. M. Polvani, J. Austin, and F. Li, 2008: The frequency and dynamics of stratospheric sudden warmings in the 21st century. *J. Geophys. Res.*, **113**, D16116, <https://doi.org/10.1029/2007JD009571>.
- , and Coauthors, 2013: On the lack of stratospheric dynamical variability in low-top versions of the CMIP5 models. *J. Geophys. Res. Atmos.*, **118**, 2494–2505, <https://doi.org/10.1002/jgrd.50125>.
- Cohen, J., and J. Jones, 2011: Tropospheric precursors and stratospheric warmings. *J. Climate*, **24**, 6562–6572, <https://doi.org/10.1175/2011JCLI4160.1>.
- , M. Barlow, P. Kushner, and K. Saito, 2007: Stratosphere-troposphere coupling and links with Eurasian land surface variability. *J. Climate*, **20**, 5335–5343, <https://doi.org/10.1175/2007JCLI1725.1>.
- Craig, R. A., and W. S. Hering, 1959: The stratospheric warming of January-February 1957. *J. Meteor.*, **16**, 91–107, [https://doi.org/10.1175/1520-0469\(1959\)016<0091:TSWJF>2.0.CO;2](https://doi.org/10.1175/1520-0469(1959)016<0091:TSWJF>2.0.CO;2).
- Garfinkel, C. I., S. B. Feldstein, D. W. Waugh, C. Yoo, and S. Lee, 2012: Observed connection between stratospheric sudden warmings and the Madden-Julian Oscillation. *Geophys. Res. Lett.*, **39**, L18807, <https://doi.org/10.1029/2012GL053144>.
- , J. J. Benedict, and E. D. Maloney, 2014: Impact of the MJO on the boreal winter extratropical circulation. *Geophys. Res. Lett.*, **41**, 6055–6062, <https://doi.org/10.1002/2014GL061094>.
- Gerber, E. P., and L. M. Polvani, 2009: Stratosphere-troposphere coupling in a relatively simple AGCM: The importance of stratospheric variability. *J. Climate*, **22**, 1920–1933, <https://doi.org/10.1175/2008JCLI2548.1>.
- Goss, M., and S. B. Feldstein, 2015: The impact of the initial flow on the extratropical response to Madden-Julian oscillation convective heating. *Mon. Wea. Rev.*, **143**, 1104–1121, <https://doi.org/10.1175/MWR-D-14-00141.1>.
- , and —, 2017: Why do similar patterns of tropical convection yield extratropical circulation anomalies of opposite sign? *J. Atmos. Sci.*, **74**, 487–511, <https://doi.org/10.1175/JAS-D-16-0067.1>.
- , —, and S. Lee, 2016: Stationary wave interference and its relation to tropical convection and arctic warming. *J. Climate*, **29**, 1369–1389, <https://doi.org/10.1175/JCLI-D-15-0267.1>.
- Hall, N., 2000: A simple GCM based on dry dynamics and constant forcing. *J. Atmos. Sci.*, **57**, 1557–1572, [https://doi.org/10.1175/1520-0469\(2000\)057<1557:ASGBOD>2.0.CO;2](https://doi.org/10.1175/1520-0469(2000)057<1557:ASGBOD>2.0.CO;2).
- Held, I. M., 1983: Stationary and quasi-stationary eddies in the extratropical troposphere. *Large-Scale Dynamical Processes in the Atmosphere*, B. J. Hoskins and R. P. Pearce, Eds., Academic Press, 127–168.
- , and M. J. Suarez, 1994: A proposal for the intercomparison of the dynamical cores of atmospheric general circulation models. *Bull. Amer. Meteor. Soc.*, **75**, 1825–1830, [https://doi.org/10.1175/1520-0477\(1994\)075<1825:APFTIO>2.0.CO;2](https://doi.org/10.1175/1520-0477(1994)075<1825:APFTIO>2.0.CO;2).
- Hendon, H. H., C. Zhang, and J. D. Glick, 1999: Interannual variation of the Madden-Julian Oscillation during austral summer. *J. Climate*, **12**, 2538–2550, [https://doi.org/10.1175/1520-0442\(1999\)012<2538:IVOTMJ>2.0.CO;2](https://doi.org/10.1175/1520-0442(1999)012<2538:IVOTMJ>2.0.CO;2).

- Holton, J. R., and C. Mass, 1976: Stratospheric vacillation cycles. *J. Atmos. Sci.*, **33**, 2218–2225, [https://doi.org/10.1175/1520-0469\(1976\)033<2218:SVC>2.0.CO;2](https://doi.org/10.1175/1520-0469(1976)033<2218:SVC>2.0.CO;2).
- , and H.-C. Tan, 1980: The influence of the equatorial quasi-biennial oscillation on the global circulation at 50 mb. *J. Atmos. Sci.*, **37**, 2200–2208, [https://doi.org/10.1175/1520-0469\(1980\)037<2200:TIOTEQ>2.0.CO;2](https://doi.org/10.1175/1520-0469(1980)037<2200:TIOTEQ>2.0.CO;2).
- Hoskins, B. J., and F. F. Jin, 1991: The initial value problem for tropical perturbations to a baro-clinic atmosphere. *Quart. J. Roy. Meteor. Soc.*, **117**, 299–317, <https://doi.org/10.1002/qj.49711749803>.
- Ineson, S., and A. Scaife, 2009: The role of the stratosphere in the European climate response to El Niño. *Nat. Geosci.*, **2**, 32–36, <https://doi.org/10.1038/ngeo381>.
- Jin, F., and B. J. Hoskins, 1995: The direct response to tropical heating in a baroclinic atmosphere. *J. Atmos. Sci.*, **52**, 307–319, [https://doi.org/10.1175/1520-0469\(1995\)052<0307:TDRTH>2.0.CO;2](https://doi.org/10.1175/1520-0469(1995)052<0307:TDRTH>2.0.CO;2).
- Jones, C., and L. M. V. Carvalho, 2006: Changes in the activity of the Madden-Julian Oscillation during 1958–2004. *J. Climate*, **19**, 6353–6370, <https://doi.org/10.1175/JCLI3972.1>.
- Kang, W., and E. Tziperman, 2017: More frequent sudden stratospheric warming events due to enhanced MJO forcing expected in a warmer climate. *J. Climate*, **30**, 8727–8743, <https://doi.org/10.1175/JCLI-D-17-0044.1>.
- Kim, B.-M., S.-W. Son, S.-K. Min, J.-H. Jeong, S.-J. Kim, X. Zhang, T. Shim, and J.-H. Yoon, 2014: Weakening of the stratospheric polar vortex by Arctic sea-ice loss. *Nat. Commun.*, **5**, 4646, <https://doi.org/10.1038/ncomms5646>.
- Kim, J., S.-W. Son, E. P. Gerber, and H.-S. Park, 2017: Defining sudden stratospheric warming in climate models: Accounting for biases in model climatologies. *J. Climate*, **30**, 5529–5546, <https://doi.org/10.1175/JCLI-D-16-0465.1>.
- Kolstad, E. W., T. Breiteig, and A. A. Scaife, 2010: The association between stratospheric weak polar vortex events and cold air outbreaks in the Northern Hemisphere. *Quart. J. Roy. Meteor. Soc.*, **136**, 886–893, <https://doi.org/10.1002/qj.620>.
- Lee, S., 1999: Why are the climatological zonal winds easterly in the equatorial upper troposphere? *J. Atmos. Sci.*, **56**, 1353–1363, [https://doi.org/10.1175/1520-0469\(1999\)056<1353:WATCZW>2.0.CO;2](https://doi.org/10.1175/1520-0469(1999)056<1353:WATCZW>2.0.CO;2).
- Limpasuvan, V., D. Thompson, and D. Hartmann, 2004: The life cycle of the Northern Hemisphere sudden stratospheric warmings. *J. Climate*, **17**, 2584–2596, [https://doi.org/10.1175/1520-0442\(2004\)017<2584:TLCOTN>2.0.CO;2](https://doi.org/10.1175/1520-0442(2004)017<2584:TLCOTN>2.0.CO;2).
- Lin, H., and G. Brunet, 2018: Extratropical response to the MJO: Nonlinearity and sensitivity to the initial state. *J. Atmos. Sci.*, **75**, 219–234, <https://doi.org/10.1175/JAS-D-17-0189.1>.
- Madden, R. A., and P. R. Julian, 1971: Detection of a 40–50 day oscillation in zonal wind in the tropical Pacific. *J. Atmos. Sci.*, **28**, 702–708, [https://doi.org/10.1175/1520-0469\(1971\)028<0702:DOADOI>2.0.CO;2](https://doi.org/10.1175/1520-0469(1971)028<0702:DOADOI>2.0.CO;2).
- Martius, O., L. M. Polvani, and H. C. Davies, 2009: Blocking precursors to stratospheric sudden warming events. *Geophys. Res. Lett.*, **36**, L14806, <https://doi.org/10.1029/2009GL038776>.
- Matsuno, T., 1971: A dynamical model of the stratospheric sudden warming. *J. Atmos. Sci.*, **28**, 1479–1494, [https://doi.org/10.1175/1520-0469\(1971\)028<1479:ADMOTS>2.0.CO;2](https://doi.org/10.1175/1520-0469(1971)028<1479:ADMOTS>2.0.CO;2).
- McLandress, C., and T. G. Shepherd, 2009: Impact of climate change on stratospheric sudden warmings as simulated by the Canadian middle atmosphere model. *J. Climate*, **22**, 5449–5463, <https://doi.org/10.1175/2009JCLI3069.1>.
- Mitchell, D. M., S. M. Osprey, L. J. Gray, N. Butchart, S. C. Hardiman, A. J. Charlton-Perez, and P. Watson, 2012: The effect of climate change on the variability of the Northern Hemisphere stratospheric polar vortex. *J. Atmos. Sci.*, **69**, 2608–2618, <https://doi.org/10.1175/JAS-D-12-021.1>.
- , L. J. Gray, J. Anstey, M. P. Baldwin, and A. J. Charlton-Perez, 2013: The influence of stratospheric vortex displacements and splits on surface climate. *J. Climate*, **26**, 2668–2682, <https://doi.org/10.1175/JCLI-D-12-00030.1>.
- Naoe, H., and Y. Matsuda, 1998: Rossby wave propagation and nonlinear effects in zonally-varying basic flows. *J. Meteor. Soc. Japan*, **76**, 385–402, [https://doi.org/10.2151/jmsj1965.76.3\\_385](https://doi.org/10.2151/jmsj1965.76.3_385).
- , —, and H. Nakamura, 1997: Rossby wave propagation in idealized and realistic zonally varying flows. *J. Meteor. Soc. Japan*, **75**, 687–700, [https://doi.org/10.2151/jmsj1965.75.3\\_687](https://doi.org/10.2151/jmsj1965.75.3_687).
- Neale, R. B., and Coauthors, 2010: Description of the NCAR Community Atmosphere Model (CAM 4.0). NCAR Tech Note NCAR/TN-485+STR, NCAR, 224 pp., [http://www.cesm.ucar.edu/models/cesm4.0/cam/docs/description/cam4\\_desc.pdf](http://www.cesm.ucar.edu/models/cesm4.0/cam/docs/description/cam4_desc.pdf).
- O'Brien, E., D. A. Stewart, and L. E. Branscome, 1994: Tropical-extratropical interactions on intraseasonal time scales in a global spectral model. *J. Atmos. Sci.*, **51**, 1244–1260, [https://doi.org/10.1175/1520-0469\(1994\)051<1244:TIOITS>2.0.CO;2](https://doi.org/10.1175/1520-0469(1994)051<1244:TIOITS>2.0.CO;2).
- Oliver, E. C., and K. R. Thompson, 2012: A reconstruction of Madden-Julian Oscillation variability from 1905 to 2008. *J. Climate*, **25**, 1996–2019, <https://doi.org/10.1175/JCLI-D-11-00154.1>.
- Richter, J. H., A. Solomon, and J. T. Bacmeister, 2014: Effects of vertical resolution and nonorographic gravity wave drag on the simulated climate in the community atmosphere model, version 5. *J. Adv. Model. Earth Syst.*, **6**, 357–383, <https://doi.org/10.1002/2013MS000303>.
- Schimanke, S., T. Spanghel, H. Huebener, and U. Cubasch, 2013: Variability and trends of major stratospheric warmings in simulations under constant and increasing GHG concentrations. *Climate Dyn.*, **40**, 1733–1747, <https://doi.org/10.1007/s00382-012-1530-x>.
- Schubert, J. J., B. Stevens, and T. Crueger, 2013: Madden-Julian Oscillation as simulated by the MPI Earth system model: Over the last and into the next millennium. *J. Adv. Model. Earth Syst.*, **5**, 71–84, <https://doi.org/10.1029/2012MS000180>.
- Schwartz, C., and C. I. Garfinkel, 2017: Relative roles of the MJO and stratospheric variability in North Atlantic and European winter climate. *J. Geophys. Res. Atmos.*, **122**, 4184–4201, <https://doi.org/10.1002/2016JD025829>.
- Simmons, A. J., J. M. Wallace, and G. W. Branstator, 1983: Barotropic wave propagation and instability, and atmospheric teleconnection patterns. *J. Atmos. Sci.*, **40**, 1363–1392, [https://doi.org/10.1175/1520-0469\(1983\)040<1363:BWPAIA>2.0.CO;2](https://doi.org/10.1175/1520-0469(1983)040<1363:BWPAIA>2.0.CO;2).
- Slingo, J., D. Rowell, K. Sperber, and E. Nortley, 1999: On the predictability of the interannual behaviour of the Madden-Julian oscillation and its relationship with El Niño. *Quart. J. Roy. Meteor. Soc.*, **125**, 583–609, <https://doi.org/10.1002/qj.49712555411>.
- Solomon, S., R. R. Garcia, F. S. Rowland, and D. J. Wuebbles, 1986: On the depletion of Antarctic ozone. *Nature*, **321**, 755–758, <https://doi.org/10.1038/321755a0>.
- Thompson, D. W. J., M. P. Baldwin, and J. M. Wallace, 2002: Stratospheric connection to Northern Hemisphere winter-time weather: Implications for prediction. *J. Climate*, **15**, 1421–1428, [https://doi.org/10.1175/1520-0442\(2002\)015<1421:SCTNHW>2.0.CO;2](https://doi.org/10.1175/1520-0442(2002)015<1421:SCTNHW>2.0.CO;2).
- Ting, M. F., and P. D. Sardeshmukh, 1993: Factors determining the extratropical response to equatorial diabatic heating anomalies. *J. Atmos. Sci.*, **50**, 907–918, [https://doi.org/10.1175/1520-0469\(1993\)050<0907:FDTERT>2.0.CO;2](https://doi.org/10.1175/1520-0469(1993)050<0907:FDTERT>2.0.CO;2).

- Vallis, G. K., 2006: *Atmospheric and Oceanic Fluid Dynamics: Fundamentals and Large-Scale Circulation*. Cambridge University Press, 745 pp.
- Webster, P. J., and H.-R. Chang, 1988: Equatorial energy accumulation and emanation regions: Impacts of a zonally varying basic state. *J. Atmos. Sci.*, **45**, 803–829, [https://doi.org/10.1175/1520-0469\(1988\)045<0803:EEAER>2.0.CO;2](https://doi.org/10.1175/1520-0469(1988)045<0803:EEAER>2.0.CO;2).
- Yoo, C., S. Feldstein, and S. Lee, 2011: The impact of the Madden-Julian Oscillation trend on the Arctic amplification of surface air temperature during the 1979–2008 boreal winter. *Geophys. Res. Lett.*, **38**, L24804, <https://doi.org/10.1029/2011GL049881>.
- , S. Lee, and S. B. Feldstein, 2012a: Arctic response to an MJO-like tropical heating in an idealized GCM. *J. Atmos. Sci.*, **69**, 2379–2393, <https://doi.org/10.1175/JAS-D-11-0261.1>.
- , —, and —, 2012b: Mechanisms of Arctic surface air temperature change in response to the Madden–Julian Oscillation. *J. Climate*, **25**, 5777–5790, <https://doi.org/10.1175/JCLI-D-11-00566.1>.
- Zhang, C., 2005: Madden-Julian oscillation. *Rev. Geophys.*, **43**, RG2003, <https://doi.org/10.1029/2004RG000158>.